

Thickness optimization in wide range quasi omnidirectional 1-D photonic structures

Victor Castillo-Gallardo^{*1,2,3}, Luis Eduardo Puente-Díaz^{1,2,3}, D. Ariza-Flores⁴, Hector Pérez-Aguilar³, W. Luis Mochán^{†2}, and Vivechana Agarwal^{‡1}

¹Centro de Investigación en Ingeniería y Ciencias Aplicadas, Universidad del Estado de Morelos, Av. Universidad 1001 Col. Chamilpa, Cuernavaca, Morelos 62209, México.

²Instituto de Ciencias Físicas, Universidad Nacional Autónoma de México, Av. Universidad S/N, Col. Chamilpa, 62210 Cuernavaca, Morelos, México.

³Facultad de Ciencias Físico Matemáticas, Universidad Michoacana de San Nicolás de Hidalgo, Av. Francisco J. Múgica S/N 58030, Morelia, Mich., México.

⁴Conacyt-Universidad Autónoma de San Luis Potosí, Karakorum 1470, Lomas 4ta Secc, San Luis Potosí, S.L.P., 78210, México.

September 18, 2020

Abstract

Porous silicon (PS) is a very versatile material for developing optical devices based on multilayer structures, since high and low porosity layers can be synthesized by simple electrochemical technique. We report the maximization of average reflectance ($R_{\text{prom}}(\lambda, \theta)$) with minimum possible thickness of PS-based mirrors with different porosity contrasts. Optimization is performed in two regions (Visible and NIR) of the electromagnetic spectrum. We employ two techniques to design the mirrors: *chirped* structures and the *stacking* of sub-mirrors. The chirped structures were found to be relatively more suitable for obtaining highly reflectivity in the visible range, while the second type of structure was more effective for obtaining high reflectivity in the IR region. Some of the optimized omnidirectional structures with less than 100 periods have been designed and experimentally demonstrated in a wide spectral range.

1 Introduction

Photonic crystal (PC)-based structures are extensively investigated due to their light controlling properties [1,2]. Photons entering a PC interact with its period-

^{*}email: victor1.1@hotmail.com

[†]email: mochan@fis.unam.mx

[‡]email: vagarwal@uaem.mx

ically varying dielectric constant and are consequently organized into photonic bands. Analogous to electrons in a crystal, their propagation will be limited by photonic band gaps (PBGs) where transmission states are forbidden. The PC shows a PBG corresponding to the electromagnetic modes which are not allowed to propagate through the structure and behaves as a perfect mirror for that range. The width of reflection spectrum is important while designing an omnidirectional mirror for different applications. The metallic mirrors are widely accepted for reflection purposes, but widespread use is limited due to their absorptive nature at the visible and near infrared frequencies. A good alternative are dielectric structures as they also provide design flexibility in terms of reflection wavelength. These properties are widely used to design various one-dimensional (1D) and two-dimensional (2D) PCs for its potential applications in optoelectronics, optical telecommunications and computing, laser technology [3, 4], and radiative cooling applications [5]. The simplest 1D PC is composed of alternating high (n_H) and low (n_L) refractive index layers (Bragg Mirror, BM). The optical thicknesses are typically chosen to be quarter-wavelength length, $n_H d_H = n_L d_L = \lambda_0/4$, at some operating wavelength λ_0 (center wavelength) to obtain a certain omnidirectional band gap. As the gap depends on the contrast of the refractive indices and the number of periods, broadband mirrors can be engineered by modulating the reflection in a broader wavelength range. One of the ways to obtain such structures has been the continuous variation of thicknesses along the depth, defined as *chirped*-type [6] structures. Additionally, broader mirrors can also be achieved by overlapping different BMs, where each one reflects around a specific central wavelength, resulting in a wider photonic band gap [7].

Till now, different deposition techniques have been used to obtain omnidirectional BM (ODBM) that operate on the visible and near infrared (Vis-NIR) range of the electromagnetic spectrum. For example, Chen et al., [8] have reported an ODBM of about 70 nm in NIR range designed with 6-pairs of $\text{TiO}_2/\text{SiO}_2$ deposited using sol-gel method. Park et al., [9] used molecular beam epitaxy to grow a stack of four pairs of GaAs/AlAs layers, followed by its conversion to a multilayer stack of $\text{GaAs}/\text{Al}_2\text{O}_3$ by selective oxidation of the AlAs layers, to obtain an ODBM with a gap from 710 to 950 nm. On the other hand, DeCorby et al., [10] fabricated mirrors by coupling multiple layers of $\text{Ge}_{33}\text{As}_{12}\text{Se}_{55}$ chalcogenide glass and polyamide-imide polymer, deposited by thermal evaporation and spin-casting respectively, to obtain 150 nm wide omnidirectional band, centered at 1750 nm wavelength. Furthermore, Jena et al., [11] used sequential asymmetric bipolar pulsed DC magnetron sputtering (for TiO_2 layers) and radio frequency magnetron sputtering (for SiO_2 layers) to generate 1DPC of $\text{TiO}_2/\text{SiO}_2$ and achieved ODBM from 592 to 668 nm. However, these techniques are expensive and require sophisticated equipment and long fabrication time. Using porous silicon (PS) is an alternative, as PS is typically fabricated by simple electrochemical etching of crystalline Si in hydrofluoric acid based electrolyte, to obtain the sponge-like nanostructure composed of Si and air in a relatively short duration of time. The generated porosity can be tuned by changing the applied current density and hence modifies the refractive index

of the resulting PS. This fact opens the possibility of designing 1DPC with PS, which seeks to control the propagation of light in a dielectric medium. The low cost and ease of obtaining porous silicon make it an excellent candidate to develop optical devices based on multilayer structures [12,13]. Although optical filters [14,15] are the most common application of porous silicon, they have been widely used as chemical sensors [16,17], waveguides [18] and photoluminescence control [19]. Recently, the study of quasi-omnidirectional Bragg mirrors has increased due to their possible application as a flat lens [20,21]. In particular, PS based dielectric optical filters, quasi-ODBM and ODBM have been extensively studied in different regions of the electromagnetic spectrum, such as ultraviolet (UV) [22], visible [23], and (NIR) [24]. Keeping in view that high values of average porosity, refractive index contrast and thickness make the multilayer structures fragile, in this work various wide band gap photonic structures have been proposed to obtain maximal average reflectance ($R_{ave}(\lambda, \theta)$) with the minimum possible thickness and low refractive index contrast.

This paper is organized as follows. Section 2 presents the development of methods used to design and calculate the reflectance spectra of the PS multilayer structures. Section 3 provides the experimental details about the fabrication of some of these structures. Section 4 presents the numerical results corresponding to different methodologies (chirped structures and sub-mirror stacks) adopted to minimize the thickness of the structure for maximal reflectance along with the experimental results and its comparison with the existing reports. The obtained experimental results revealed an enhancement in the quasi omnidirectional band gap (0-60°) by a factor of approximately 2 with half the structure physical thickness in both the configurations, compared to the last reported works [25,26]. Finally, the conclusions of this work are presented in Section 5.

2 Theoretical analysis

In the analysis of the propagation of the electromagnetic field through multilayer systems, it is common to employ the transfer matrix method (put the reference). Under the consideration that the system only varies along the z axis, the transfer matrix is $M(z_2, z_1)$ a 2x2 matrix that relates the components of the electric field E_{\parallel} and the magnetic field H_{\parallel} parallel to the xy plane, and normal to the axis of the structure, evaluated at any two points z_2 and z_1

$$\begin{pmatrix} E_{\parallel} \\ H_{\parallel} \end{pmatrix}_{z_2} = M(z_2, z_1) \begin{pmatrix} E_{\parallel} \\ H_{\parallel} \end{pmatrix}_{z_1}.$$

Many equivalent formulations have been proposed to obtain M [26–28]. Here we use a recently developed formalism to calculate the reflectance of large multilayer systems proposed by Puente-Díaz, et al [29], since we need a reliable and stable tool to design an optimized structure through a minimization procedure that requires the calculation of complete spectra for all sets of design parameters. The development of M is shown in the supplementary information. Therefore,

the explicit expressions for the optical coefficients are:

$$r = \mp \frac{Z_0 \tilde{M}_{11} + \tilde{M}_{12} - Z_0 Z_s \tilde{M}_{21} - Z_s \tilde{M}_{22}}{Z_0 \tilde{M}_{11} - \tilde{M}_{12} - Z_0 Z_s \tilde{M}_{21} + Z_s \tilde{M}_{22}}, \quad (1) \quad \boxed{\text{rBloch}}$$

and

$$t = \frac{2Z_\alpha}{Z_0 \tilde{M}_{11} - \tilde{M}_{12} - Z_0 Z_s \tilde{M}_{21} + Z_s \tilde{M}_{22}}, \quad (2) \quad \boxed{\text{tBloch}}$$

where the upper sign – in Eq. (1) and the subscript $\alpha = s$ in Eq. (2) are chosen for the case of TE polarization, while the lower sign + and the subscript $\alpha = 0$ correspond to TM polarization, respectively. Furthermore, \tilde{M}_{ij} are the elements of the transfer matrix. As usual, the reflectance is given by $R = |r|^2$ and the transmittance by $T = \beta |t|^2$ with $\beta = Z_0/Z_s$ for the case of TE polarization and $\beta = Z_s/Z_0$ for the case of TM polarization. Additionally, complex refractive indices of the porous layers in the simulations were obtained by Bruggeman effective medium theory, which has been reported to adequately reproduce the PS optical parameters [16, 30, 31].

After the next section, two techniques are developed to design multilayer photonic structures. In the first, the wavelength (λ_j), at which the j -th period of the structure is designed, is modulated by an increasing function. This can be as simple or complex as you like. The proposed function was optimized with the Minuit module of PDL (Perl Data Language) [32]. The other technique for proposing highly reflective structures over a wide region of the electromagnetic spectrum is to stack sub-mirrors tuned to different wavelengths. For each sub-mirror the dispersion relation is analyzed.

3 Experimental details

Some of the proposed photonic structures were synthesized through anodic etching of a (100) oriented, p-type Boron doped, crystalline Si wafer with resistivity 0.002-0.005 $\Omega\cdot\text{cm}$, under galvanostatic conditions [33, 34]. Electrochemical anodization process was performed at room temperature, with an electrolyte of aqueous HF (48% of wt) and ethanol (99.9% of wt) in 1:1 volumetric proportion, respectively. With this electrolyte, the minimum and maximum porosities that can be obtained are 35% and 76% (gravimetrically obtained), using current densities of 0.5 and 305 mA/cm^2 , respectively. However, it is not desirable to use very high porosity contrasts due to structure fragility and electrolyte diffusivity problems [35]. For this reason, the current densities were chosen as 35 and 305 mA/cm^2 , with corresponding porosities of 51% and 76%, respectively. The calibration curves were acquired through a gravimetric technique as follows: single layers of porous silicon were synthesized under similar conditions and were weighed (m_i) before (m_1) and after (m_2) the electrochemical attack, and after dissolving the already formed porous silicon layer (m_3), to calculate the porosity as $p = (m_1 - m_2)/(m_1 - m_3)$ [36]. Etching rate of PS was

obtained by re-synthesizing individual layers under similar conditions and measuring their thicknesses through scanning electron microscopy (SEM). The absolute reflectivity measurements were carried out with a Perkin Elmer Lambda 950 UV/Visible spectrophotometer with a variable angle universal reflectance accessory (URA) for different incident angles $\theta_i = 10^\circ, 20^\circ, 30^\circ, 40^\circ, 50^\circ$ and 60° using non-polarized light. The maximum and minimum values of θ_i were constrained by the angular range of the equipment accessory URA.

4 Results and discussion

This section presents the comparison of the calculated and measured reflectance spectra at different incidence angles in the regions of interest. In the first subsection, the design and optimization of $R_{ave}(\lambda, \theta)$ of *chirped* photonic structures is presented, and next subsection the design of the structure is analyzed through sub-mirrors stacks.

4.1 Chirped-type Bragg mirrors

The generic form of the expression that modulates the design of photonic structure is:

$$\lambda_j = \lambda_{\min} + (\lambda_{\max} - \lambda_{\min}) f(x_j), \quad (3) \quad \boxed{\text{Dis}}$$

where λ_{\min} , λ_{\max} and λ_j correspond to the minimum, maximum, and design wavelengths to which the j -th period is tuned, respectively, and $f(x_j)$ represents any normalized function that modulates the thickness. Here $x_j = \frac{j}{N_p}$ being j the j -th period and N_p the total number of periods that the structure will contain. Only restriction for $f(x_j)$ is that it has to be an increasing function, due to the high absorption of PS in the ultraviolet region which decreases in the visible and becomes negligible in the near infrared. So, the first periods are syntonized in the UV-Vis regions. This work shows the analysis of following functions:

$$f_1(x) = x^\alpha, \quad (4) \quad \boxed{\text{F1}}$$

$$f_2(x) = A(x^\alpha + x^\beta) \quad (5) \quad \boxed{\text{F2}}$$

and

$$f_3(x) = Ax^\alpha(1-x) + x^\beta, \quad (6) \quad \boxed{\text{F3}}$$

where α , β and A are parameters to optimize. The function f_1 (Eq. (4)) represents the simplest profiles. The restrictions for the values α are that they must be positive and they must not be extremely large or small. In these cases, mirrors that reflect in λ_{\min} or λ_{\max} , respectively, will be obtained. Eq. (5) is formed by the average of two functions of type f_1 with different powers. The function f_3 (Eq. (6)) was designed so that the first and second additions predominate the short and long wavelengths, respectively. The $R_{ave}(\lambda, \theta)$ of the structures is calculated in the wavelength range from 350 to 1400 nm and from 0 to 90° angle of incidence. The optimized parameters using a porosity

Table 1: Design parameters obtained after the optimization of functions (Eqs. (4) - (6)) for maximum average reflectance and minimum thickness

Function	λ_0 (μm)		Function parameters			Periods N_p	Thickness (μm)	R_{Ave} %
	Min	Max	α	β	A			
f_1	0.25	1.4	0.24	----	----	222	86.1	89
f_2	0.40	1.4	0.37	1.06	0.50	102	35.9	88
f_3	0.32	1.4	1.23	0.54	0.18	63	21.6	89

contrast of 51/76% are shown in Table 1 and in the supplementary information they appear for the porosity contrasts of 30/76% and 42/76%.

According to the values shown in table I, the structure (named as ST-A) that has the maximum average reflectance with the minimum thickness is the one designed with the function f_3 (Eq. (6)). Thus, the first and last periods are tuned to 320 and 1400 nm, respectively. The complete distribution of the periods is presented in Fig. I(a). To verify that the values obtained are optimal, in Fig. I(b), the average reflectances of the photonic structures designed with different parameters are mapped and, indeed, the values are in the area where $R_{\text{ave}}(\lambda, \theta)$ is maximum. Here, the parameters λ_{\min} , λ_{\max} , β and A were adjusted, while N_p and α varied from 30 to 200 periods and from 0.4 to 1.3, respectively. The calculated reflectance, $R(\lambda, \theta)$, of the photonic structure is shown in Fig I(c). Here, the wavelength and incidence angle cover the ranges from 350 to 1400 nm, and from 0° to 90° , respectively. Calculations indicate that the structure has a localized omnidirectional band gap from 1000 to 1200 nm, taken with a reflectance greater than 95%. Due to experimental limitations, reflectance spectra for non polarized light are shown in all results. In Fig. I(d), the calculated and measured reflectance is compared at 10° , 20° , 30° , 40° , 50° and 60° of incidence. In this angular range, the structure has a quasi-omnidirectional band gap ($R(\lambda, \theta) > 95\%$) located from 980 to 1340 nm. The numerical and experimental spectral line shapes at different angles are in good agreement. For wavelengths greater than 700 nm and lying between 10° to 40° of incidence angle, the difference in spectra is less than 5%. For angles of incidence greater than 40 degree, although their characteristics are similar, the measured spectrum demonstrates relatively less reflectance than calculated reflectance. This difference can be attributed, in part, to the scattering of light between each of the actual interfaces, which generally have some roughness [26,37].

Due to the absorptive nature of Si in the UV and visible region, it is relatively difficult to design porous silicon omnidirectional mirrors in that region. However, in the IR region, it is relatively easy to obtain highly reflective and even omnidirectional photonic structures over a wide range. Therefore, the average reflectance was optimized using the function f_1 (Eq. (4)) in the region of 850 to 3000 nm. It was found that the best value for α is 1.2 and the minimum thickness is 60.4 μm , distributed in 90 periods. The complete design of the structure (named as ST-B) is graphed in Fig. 2(a). In Fig 2(b) the average reflectance of structures designed with different values of α and N_p is mapped.

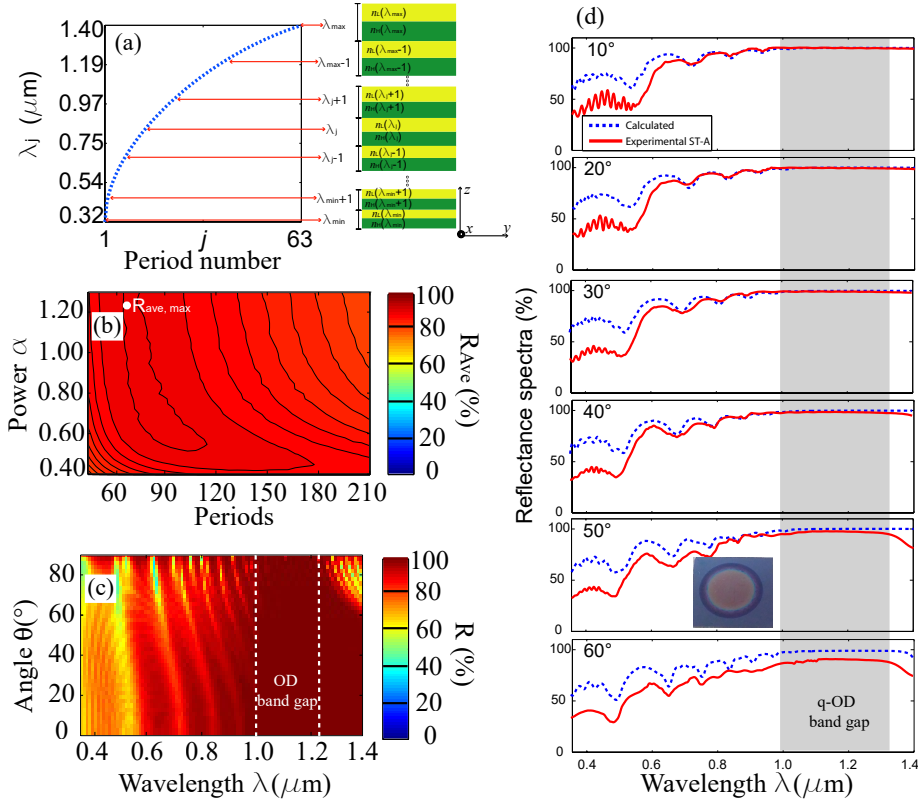


Figure 1: (a) Distribution of λ_j in the j -th period for the design of the 63-period multilayer structure. (b) Mapping of the average reflectance of the structures designed with different values of α and N_p parameters. It is verified that the parameters obtained during the optimization are adequate ($\alpha = 1.23$ and $N_p = 63$). (c) Mapping the calculated reflectance for non polarized light of the designed structure with the optimized values. (d) Comparison of reflectance spectra calculated and measured at different angles of incidence. The gray band indicates the region in which the reflectance is greater than 95%. Inset shows the top view photograph of the synthesized structure.

Fig2

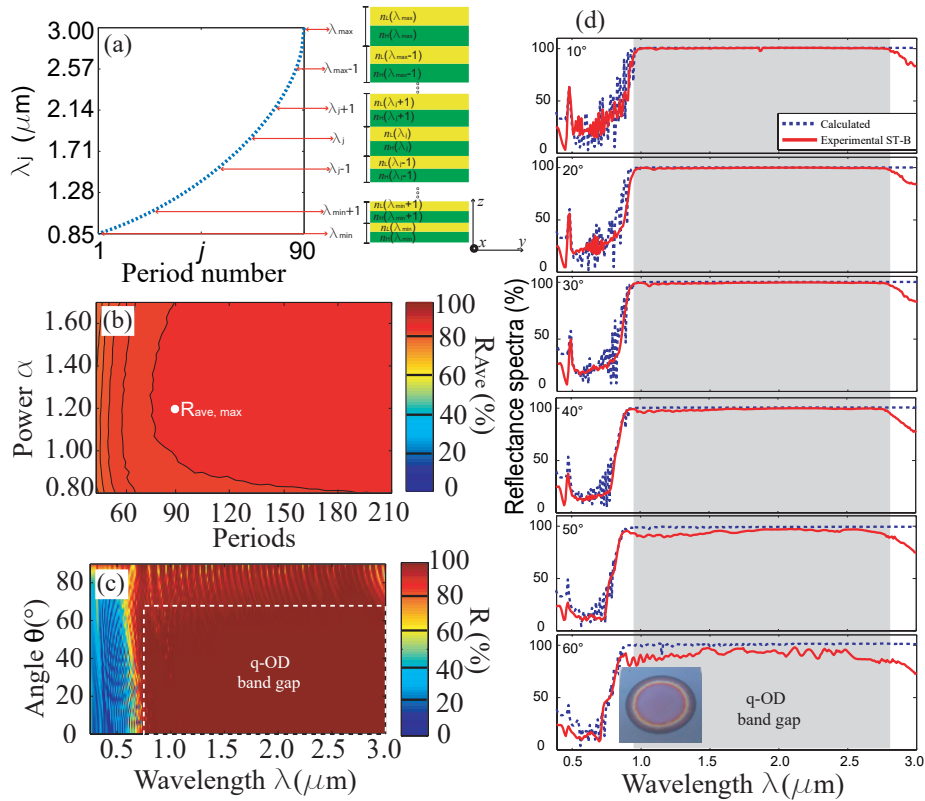


Figure 2: (a) Distribution of λ_j in the j -th period modulated by the optimization of the function f_1 for the design of the multilayer structure of 90 periods. (b) Mapping of the average reflectance of the structures designed with different values of the α and N_p parameters. The optimized parameters are $\alpha = 1.2$ and 90 periods. (c) Mapping the calculated reflectance of the designed structure with the optimized values for non polarized light. (d) Comparison of reflectance spectra calculated and measured at different angles of incidence. The gray band indicates the region in which the reflectance is greater than 95%. Inset there is a photograph of the synthesized structure.

Fig3

As in the previous case, the optimized parameters are within the zone of maximum average reflectance. The reflectance calculation shows that this structure has a wide quasi-omnidirectional gap that goes from 850 to 3000 nm and from 0° to 70° of incidence; the corresponding contour plot is shown in Fig. 2(c) and its average reflectance between 850-3000nm is greater than 95%. The measured and calculated reflectance spectra have very similar characteristics as shown in Fig 2(d). The synthesized PS multilayered 1D photonic structure has a quasi omnidirectional (from 0° to 60°) band gap of approximately 1800 nm. The difference between the calculated and measured spectra at the longer wavelengths can be attributed to a thickness gradient along the depth, which is more pronounced in the lower layers due to the restricted diffusivity of the electrolyte through the structure itself [38, 39] and interface roughness.

4.2 Photonic structure with sub-mirrors stacking

Another technique to design Bragg mirrors in a wide range of the electromagnetic spectrum is by stacking sub-mirrors at different wavelengths [?, 25, 40]. Such grouping must meet the condition imposed by the dispersion relation, $\cos KD = \frac{1}{2}\text{Tr } M$, where D is the period, which corresponds to the actual thickness of the sub-mirror, $\pm K$ represents a 1D Bloch's vector corresponding to a wave that propagates along z -direction [27, 41, 42], and Tr denotes the trace. This equation is bounded by the minimum and maximum values that the cosine function can take. Furthermore, if the value of $|\text{Tr}(M)|$ is > 2 , it indicates that this frequency will not be able to propagate through the structure.

The ideal stack of sub-mirrors would be that PBG of the j -th mirror begins at the edge of the PBG of the $j - 1$ -th mirror, until the desired interval has been covered. However, this arrangement does not give the maximum average reflectance due to the decrease in the reflectance at each intersection of the two PBGs. On the other hand, the number of periods of each sub-mirror is an important parameter due to its direct dependence on the magnitude and width of the photonic band gap. As the structures were synthesized using porous silicon, it is essential to minimize the number of periods corresponding to the visible region sub-mirrors. Also, in the supplementary information we show the reflectance calculations for structures composed of sub mirrors with a constant number of periods, in these cases ODBMs are not obtained. For these reasons, the number of periods for each mirror was chosen as follows: for design wavelengths less than 500 nm ($\lambda_D < 500$ nm), one period, for $500 < \lambda_D < 650$ nm, two periods , for $650 < \lambda_D < 800$ nm, three, and for $\lambda_D > 800$ nm, the number of periods was variable (Fig. 3(a)).

Therefore, in this work the overlap percentage of the PBGs of the first and second mirror, second and third mirror, and so on, is also optimized. Fig 3(b) shows the optimization results in terms of maximum average reflectance with respect to the PBG overlap at different sub-mirror periods, keeping them fixed (3, 4) or variable (1, 2 and 3) for $\lambda < 500$ (1 period), $500 < \lambda < 650$ nm (2 periods), $650 < \lambda < 800$ nm (3 periods) and $\lambda > 800$ (3, 6 periods). For example, the calculations corresponding to the reflectance spectra of the structures formed

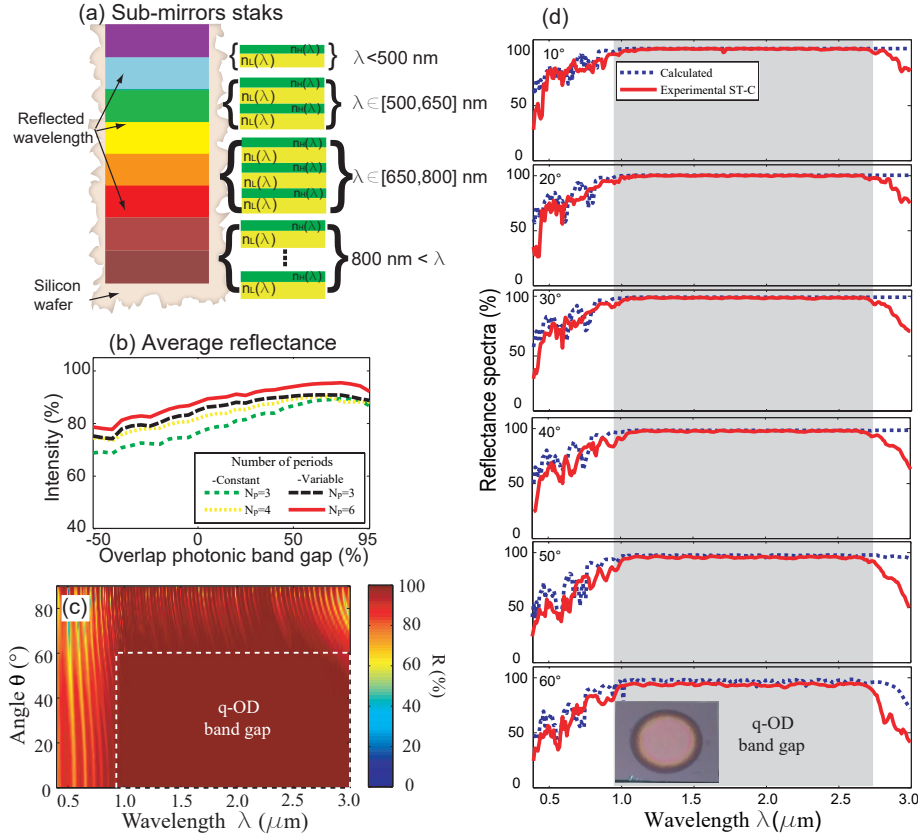


Figure 3: (a) Diagram showing the distribution of sub-mirrors and the corresponding number of periods in a PS multilayer. (b) Maximization of the average reflectance as a function of the overlap photonic band gap for the structures formed by sub-mirrors with a fixed number of periods (3 and 4), and for structures with the design of (a) using 3 and 6 periods for the tuned sub-mirrors in $\lambda > 800 \text{ nm}$. (c) Mapping the calculated reflectance of the designed structure with the optimized values for non polarized light. (d) Comparison of reflectance spectra calculated and measured at different angles of incidence. The gray band indicates the region in which the reflectance is greater than 95%. Inset shows the top view photograph of the synthesized structure.

Fig4

using sub-mirrors with constant periods (3 and 4) revealed a lower average reflectance as compared to the structure formed with variable periods. The 1D photonic structure with the highest average reflectance (named as ST-C) is the one designed with variable periods and contemplates 6 periods for each sub-mirror in the NIR region. In the optimized structure designed for 400-3000 nm range, the photonic band gap overlap is around 78%, thickness is 41.5 μm and the average reflectance is 95.3%, when the electromagnetic waves are incident from 0° to 89°. The optimized photonic structure is made up of 18 sub-mirrors tuned to the following wavelengths 400, 460, 510, 570, 640, 720, 810, 910, 1020, 1150, 1290, 1450, 1630, 1830, 2060, 2320, 2610 and 2860 nm with periods of 1 (400, 460 nm), 2(510, 570, 640 nm), 3 (720 nm) and 6 (810 nm and above).

The reflectance mapping shown in Fig 3(c) reveals a quasi omnidirectional band gap from 950 to 2900 nm, taking into account 0° to 60° of incidence. It is also observed that at incidence angles >70°, for long wavelengths the reflectance decreases and has oscillations, which are attributed to the greater penetration of the electromagnetic field within the structure, as shown by Puente-Díaz, et al [29]. Furthermore, in supplementary information we show the transfer matrix trace calculations as a function of the wavelength and the incidence angle for the ST-C photonic structure using the TE and TM polarization. In Fig 3(d) the calculated and measured reflectance corresponding to the structure ST-C, at different angles of incidence is compared. Although, the quasi omnidirectional band gap of the synthesized structure is slightly less than that calculated (located from 950 to 2750 nm), the measured PBG is almost twice as compared to the recently reported similar structures ([25, 26]).

Finally, table 2 shows some porous silicon based ODBMs designed to operate in the NIR region and the width of the omnidirectional band gap is compared with the structures analyzed in the present study. The table reveals that the porous silicon based structures ST-B and ST-C have the widest gap width, being 1.8 times greater than recently reported works.

Table 2: Summary of the development in porous silicon based ODBMs designed in the NIR region.

Reference	Year	ODBM range (nm)	ODBM width (nm)
Bruyant, et al [24].	2003	1100-1440	340
Xifre-Pérez, et al [43].	2004	1297-1615	318
Estevez, et al [14].	2009	950-1456	506
Chavez, et al [26].	2020	1000-2000	1000
This article	ST-A	980-1340	360
	ST-B	980-2780	1800
	ST-C	950-2750	1800

5 Conclusion

We have demonstrated the formation of highly reflective PS multilayer photonic structures optimized using two types of design techniques for maximal reflectance and minimal thickness in the NIR region. With *chirped*-type Bragg mirrors, two regions of the electromagnetic spectrum were analyzed. The first region (350nm - 1400 nm), optimized through an increasing function resulted in an average reflectance $> 85\%$ with the quasi omnidirectional PBG of 360 nm centered at 1160 nm (980-1340 nm) for the angular range 0-60° and more than 50% of reflectance from 550-980nm. The second structure was designed for 850-3000 nm wavelength range and the synthesized structure with optimized parameters resulted in the average reflectance of 91% with q-OD bandgap from 980 to 2780 nm and a thickness of 60.4 μm . The other design technique consisting of sub-mirrors stacks (designed at different wavelengths), was optimized for maximum average reflectance with respect to the percentage overlap of the PBG for each sub-mirror. A multilayer structure using the optimized parameters with sub-mirrors stack method was obtained with the average reflectance of 95% and a thickness of 41.5 μm . Furthermore, this structure revealed a 1800 nm q-OD PBG, centered at 1850 nm, in angular range 0-60°. Therefore, this second technique was found to be better due to the decreased thickness (by a factor of 1.5) of the framework and increased average reflectance. Additionally, the analysis techniques developed here can be used to optimize reflectance with other refractive index contrasts in PS multilayers or different other systems composed of other types of materials. Such proposed structures could be used as mirrors for solar concentrators, flat focusing reflectors, thermal regulators, or, if defects are included, as filters or remote chemical/biosensors with a wide angular independent response.

Acknowledgments

This work was partially supported by Consejo Nacional de Ciencia y Tecnología through grant No. **256243** and Cátedras Conacyt program 1577.

References

- Joannopoulos2008**
 - [1] J. D. Joannopoulos et al., *Photonic Crystals: Molding the Flow of Light*, Princeton University Press, New Jersey (2008).
- Goyal2018**
 - [2] A. K. Goyal et al., Porous photonic crystal structure for sensing applications, *J. Nanophotonics* **12**(4), 040501 (2018).
- Lopez2013**
 - [3] C. López, Materials aspects of photonic crystals, *Adv. Mater.* **15**, 1679–1704 (2013).
- Masaya2010**
 - [4] N. Masaya, Manipulating light with strongly modulated photonic crystals, *Rep. Prog.Phys.* **73** 096501, (2010).

- Kumar2020**
- [5] A. K. Goyal, A. Kumar, Recent advances and progresses in photonic devices for passive radiative cooling application: a review, *J. Nanophoton.* **14(3)** 030901 (2020) <https://doi.org/10.1117/1.JNP.14.030901>
- Zipock1997**
- [6] R. Szipöcs and A. Koházi-Kis, Theory and design of chirped dielectric mirrors, *Appl. Phys. B* **65**, 115 (1997), doi:10.1007/s003400050258
- Xifre2009**
- [7] Xifre-Perez, *Appl Phys B*, **95**: 169-172 (2009)
- Chen1999**
- [8] K.M. Chen, A.W. Sparks, H.-C. Luan, D.R. Lim, K.Wada, L.C. Kimerling, SiO₂/TiO₂ omnidirectional reflector and microcavity resonator via the sol-gel method, *Appl. Phys. Lett.* **75** 3805–3807, (1999).
- Park2003**
- [9] Y. Park, Y.-G. Roh, C.-O. Cho, H. Jeon, M.G. Sung, J.C. Woo, GaAs-based near-infrared omnidirectional reflector, *Appl. Phys. Lett.* **82** (2003) 2770–2772.
- DeCorby2005**
- [10] R. G. DeCorby, H. T. Nguyen, P. K. Dwivedi, and T. J. Clement, Planar omnidirectional reflectors in chalcogenide glass and polymer, *Opt. Express* **13**, 6228-6233 (2005)
- Jena2016**
- [11] S. Jena, R.B. Tokas, S. Tripathi, K.D. Rao, D.V. Udupa, S. Thakur, N.K. Sahoo Influence of oxygen partial pressure on microstructure, optical properties, residual stress and laser induced damage threshold of amorphous HfO₂ thin films *Journal of Alloys and Compounds*, Volume 771, 2019, pp. 373-381
- Xifre2015**
- [12] Xifré-Pérez E., Ferré-Borrull J., Pallarés J., and Marsal L. F. Methods, Properties and Applications of Porous Silicon, *Electrochemically Engineered Nanoporous Materials*, Springer Series in Materials Science 220, Ch.2, (2015).
- Pavesi2000**
- [13] Bisi O., Stefano Ossicini, and Pavesi L. Porous silicon: a quantum sponge structure for silicon based optoelectronics, *Surface Science Reports* **38** 1-126, (2000).
- Estevez2009**
- [14] Estevez J. O., Arriaga J., Méndez Blas A., and Agarwal V. Enlargement of omnidirectional photonic band gap in porous silicon dielectric mirrors with a Gaussian profile refractive index. *Applied Physics Letters*, **94**, 061914, (2009).
- Ariza2014**
- [15] Ariza-Flores D., Pérez-Huerta J.S., Kumar Y., Encinas A., and Agarwal V. Design and optimization of antireflecting coatings from nanostructured porous silicon dielectric multilayers. *Solar Energy Materials & Solar Cells*, **123** 144-149, (2014).
- Giussepppe2011**
- [16] Ruminski A.M., Barillaro G., Chaffin C., and Sailor M. J., Internally Referenced Remote Sensors for HF and Cl₂ Using Reactive Porous Silicon Photonic Crystals. *Adv. Funct. Mater.*, **21**: 1511-1525, (2011).

- Agarwal2018** [17] Karthik T.V.K., Martinez L., and Agarwal V. Porous silicon ZnO/SnO₂ structures for CO₂ detection. *Journal of Alloys and Compounds*, **731** 853-863, (2018).
- Hussel1997** [18] C.P. Hussell, R.V. Ramaswamy, *IEEE Photonics Technol. Lett.* **9**, 636, (1997).
- Antunez2014** [19] Antunez E.E., Estevez J.O., Campos J., Basurto-Pensado M.A., and V. Agarwal V. Formation of photoluminescent n-type macroporous silicon: Effect of magnetic field and lateral electric potential. *Physica B* **453** 34–39, (2014).
- Kozar2017** [20] A. V. Kozar, S. V. Marchenko and P. Y. Shestakov, "Focusing and defocusing of reflected light beams from chirped dielectric layered structure," 2017 Days on Diffraction (DD), St. Petersburg, pp. 200-204, (2017).
- Cheng2018** [21] Yu-Chieh Cheng and Kestutis Staliunas, Near-field flat focusing mirrors, *Applied Physics Reviews* 5, 011101 (2018).
- Jimenez2020** [22] Jiménez-Vivanco M. R., García G., Carrillo J., Agarwal V., Díaz-Becerril T., Doti R., Faubert J., and Lugo J. E. Porous Si-SiO₂ based UV Microcavities. *Scientific Reports* **10**: 2220, (2020).
- Ariza2012** [23] Ariza-Flores A. D., Gaggero-Sager L. M., and Agarwal V. White metal like omnidirectional mirror from porous silicon dielectric multilayers. *Appl. Phys. Lett.*, 101(3):031119, (2012).
- Bryant2003** [24] Bryant A., Lerondel G., Reece P. J., and Gal M. All-silicon omnidirectional mirrors based on one-dimensional photonic crystals. *Appl. Phys. Lett.*, 82(19):3227-3229, (2003).
- DeRio2018** [25] Estrada-Wiese, D., del Río-Chanona, E.A. & del Río, J.A. Stochastic optimization of broadband reflecting photonic structures. *Sci Rep* **8**, 1193 (2018).
- Chavez2020** [26] B. A. Chavez-Castillo, J. S. Pérez-Huerta, J. Madrigal-Melchor, S. Amador-Alvarado, I. A. Sustaita-Torres, V. Agarwal, and D. Ariza-Flores, A wide band porous silicon omnidirectional mirror for the near infrared range, *Journal of Applied Physics*, **127**, 20, (2020).
- Mochan1987** [27] Mochán W. L., del Castillo-Mussot M., and Barrera Rubén G. Effect of plasma waves on the optical properties of metal-insulator superlattices. *Phys. Rev. B*, 35(3):1088-1098, (1987).
- Ortiz2020** [28] Leandro L. Missoni, Guillermo P. Ortiz, María Luz Martínez Ricci, Victor J. Toranzos, W. Luis Mochán, Rough 1D photonic crystals: A transfer matrix approach, *Optical Materials*, **109**, 110012 (2020).

- Puente2020** [29] Luis Eduardo Puente-Díaz, Víctor Castillo-Gallardo, Guillermo P. Ortiz, José Samuel Pérez-Huerta, Héctor Pérez-Aguilar, Vivechana Agarwal, W. Luis Mochán, Stable calculation of optical properties of large non-periodic dissipative multilayered systems, *Superlattices and Microstructures*, **145**, 106629, (2020).
- Pap2006** [30] Pap Andrea Edit, Kordás Krisztián, Vähäkangas Jouko, Uusimäki Antti, Leppävuori Seppo, Pilon Laurent, and Szatmári Sándor. Optical properties of porous silicon. part iii: Comparison of experimental and theoretical results. *Optical Materials*, 28(5):506-513, (2006).
- Estrada2018** [31] D. Estrada-Wiese and J. A. del Río, Refractive index evaluation of porous silicon using Bragg reflectors. *Revista mexicana de física*, **64**(1), 72-81, (2018).
- minuit** [32] James F. and Winkler M. Minuit user's guide. CERN, Geneva, (2004).
- Canham90** [33] Canham L. T. Silicon quantum wire array fabrication by electrochemical and chemical dissolution of wafers. *Appl. Phys. Lett.*, 57(**10**):1046-1048, (1990).
- Escencia07** [34] Escencia J. and Agarwal V. Effect of duty cycle and frequency on the morphology of porous silicon formed by alternating square pulse anodic etching. *Phys. Status Solidi (c)*, 4(**6**):2039-2043, (2007).
- Ariza2011** [35] A. David Ariza-Flores, L M Gaggero-Sager and V Agarwal, Effect of interface gradient on the optical properties of multilayered porous silicon photonic structures, *J Phys D: Appl Phys*, 44(15), 155102 (2011)
- Brugeman2006** [36] Andrea Edit Pap, Krisztián Kordás, Jouko Vähäkangas, Antti Uusimaki, Seppo Leppävuori, Laurent Pilon, and Sandor Szatmári. Optical properties of porous silicon. part iii: Comparison of experimental and theoretical results. *Optical Materials*, 28(**5**):506-513, (2006).
- Theiss1994** [37] W. Theiß, R. Arens-Fischer, M. Arntzen, M.G. Berger, S. Frohnhoff, S. Hilbrich, and Wernke M. Probing optical transitions in porous silicon by reflectance spectroscopy in the near infrared, visible and UV. *MRS Proceedings*, 358:435, (1994).
- Negro2003** [38] L. Dal Negro, C. J. Oton, Z. Gaburro, L. Pavesi, P. Johnson, A. Lagendijk, R. Righini, M. Colocci, and D. S. Wiersma. Light Transport through the Band-Edge States of Fibonacci Quasicrystals. *Phys. Rev. Lett.* **90**, 055501, (2003).
- Vincent1993** [39] G. Vincent. Optical properties of porous silicon superlattices *Appl. Phys. Lett.* **64**, 2367 (1994).
- Agarwal2003** [40] V. Agarwal and J. A. del Río, Tailoring the photonic band gap of a porous silicon dielectric mirror, *Applied Physics Letters* **82**, 1512 (2003).

- Mochan1988** [41] Mochán W. L. and del Castillo-Mussot M. Optics of multilayered conducting systems: Normal modes of periodic superlattices. *Phys. Rev. B*, **37**(12):6763-6771, (1988).
- Perez2018** [42] Pérez-Huerta J. S., Ariza-Flores D., Castro-García R., Mochán W. L., Ortiz G. P., and Agarwall V. Reflectivity of 1D photonic crystals: A comparison of computational schemes with experimental results. *Int. J. Mod. Phys. B*, **32**(11):1850136, (2018).
- Xifre2005** [43] E. Xifré-Pérez, L. Marsal, J. Pallarés, and J. Ferré-Borrull, “Porous silicon mirrors with enlarged omnidirectional band gap,” *J. Appl. Phys.* **97**, 064503 (2005).
- Estevez2005** [44] Estevez J. O., Arriaga J., Méndez Blas A., and Agarwal V. Omnidirectional photonic band gaps in porous silicon based mirrors with a Gaussian profile refractive index. *Appl. Phys. Lett.* **93**:191915, (2005).